Electronic Band Offset Determination of Oxides Grown by Atomic Layer Deposition on Silicon

Edris Khorani, Christoph A. Messmer, Sophie L. Pain, Tim Niewelt, Brendan F. M. Healy, Ailish Wratten, Marc Walker, Nicholas E. Grant, and John D. Murphy

***Abstract*—Minimizing electrical losses at metal/silicon interfaces in high efficiency single-junction silicon solar cells requires the use of carrier-selective passivating contacts. The electronic barrier heights at the insulator/silicon interface are necessary for calculating the probability of quantum tunnelling of charge carriers at these interfaces. Thus, precise knowledge of these parameters is crucial for the development of contact schemes. Using a photoemission-based method, we experimentally determine the electronic band offsets of Al_2O_3, HfO_2 and SiO_2 layers grown by atomic layer deposition (ALD) on silicon. For Al_2O_3/Si, we determine a valence band offset (ΔE_V) and conduction band offset (ΔE_C) of 3.29 ± 0.07 eV and 2.24 ± 0.13 eV, respectively. For HfO_2/Si, ΔE_V and ΔE_C are determined as 2.67 ± 0.07 eV and 1.81 ± 0.21 eV, whilst for SiO_2/Si, ΔE_V and ΔE_C are 4.87 ± 0.07 eV and 2.61 ± 0.12 eV, respectively. Using technology computer-aided design (TCAD) simulations, we incorporate our experimental results to estimate the contact resistivity that would be attained at various dielectric layer thicknesses. We find that for achieving the 100 mΩ.cm^2 contact resistivity benchmark, Al_2O_3 layers should be no thicker than 1.65 nm for a p-type polysilicon-based hole-selective contact, assuming hole tunnelling masses taken from the literature. Correspondingly, for HfO_2 and SiO_2, an upper limit of 1.4 nm is determined as the thickness threshold in order to utilize these ALD-grown layers for contacts in high-performance silicon photovoltaics.**

This work was supported by the Engineering and Physical Sciences Research Council (EPSRC) Charged Oxide Inversion Layer (COIL) solar cell project (EP/V037749/1) and the Leverhulme Trust (RPG-2020-377). This work was partially supported by the German Federal Ministry for Economic Affairs and Climate Action under contract no. 03EE1031A and no. 03EE1031B (PaSoDoble). Sophie L. Pain and Ailish Wratten were supported by EPSRC Doctoral Training Partnership studentships (EP/R513374/1). Marc Walker acknowledges financial support from the EPSRC-funded Warwick Analytical Science Centre (EP/V007688/1).

Edris Khorani, Sophie L. Pain, Brendan F. M. Healy, Ailish Wratten, Nicholas E. Grant and John D. Murphy are with the School of Engineering, University of Warwick, Coventry CV4 7AL, U.K. (email: edris.khorani@warwick.ac.uk; sophie.l.pain@warwick.ac.uk; brendan.healy@warwick.ac.uk; ailish.wratten@warwick.ac.uk; nicholas.e.grant@warwick.ac.uk; john.d.murphy@warwick.ac.uk).

Christoph A. Messmer is with the Fraunhofer Institute for Solar Energy Systems ISE, 79110 Freiburg, Germany, and also with the Institute for Sustainable Systems Engineering, University of Freiburg, 79110 Freiburg, Germany, and also with the Laboratory for Photovoltaic Energy Conversion, Department of Sustainable Systems Engineering (INATECH), University of Freiburg, Emmy-Noether-Straße 2, 79110 Freiburg, Germany (email: christoph.alexander.messmer@ise.fraunhofer.de).

Tim Niewelt is with the School of Engineering, University of Warwick, Coventry CV4 7AL, U.K., also with the Fraunhofer Institute for Solar Energy Systems ISE, 79110 Freiburg, Germany, and also with the Institute for Sustainable Systems Engineering, University of Freiburg, 79110 Freiburg, Germany, and also with the Laboratory for Photovoltaic Energy Conversion, Department of Sustainable Systems Engineering (INATECH), University of Freiburg, Emmy-Noether-Straße 2, 79110 Freiburg, Germany (email: tim.niewelt@warwick.ac.uk).

Marc Walker is with the Department of Physics, University of Warwick, Coventry CV4 7AL, U.K. (email: m.walker@warwick.ac.uk).

***Index Terms*—Aluminum Oxide (Al_2O_3), Atomic layer deposition (ALD), Band offset, Carrier-selective passivating contacts, Hafnium oxide (HfO_2), Silicon, Silicon dioxide (SiO_2).**

I. INTRODUCTION

ACCOUNTING for over 95% of commercial production, crystalline silicon solar cells continue to lead in the photovoltaics (PV) landscape and remain as a prominent alternative to non-renewable energy sources [1]. Currently, the bulk of this market is led by architectures that incorporate metal/Si interfaces for electrode formation [2], [3]. Avoiding this type of interface is widely accepted as the strategy towards higher performance silicon solar cells.

Due to the high density of electronically active states that arise from direct contact of metals on silicon, photogenerated charge carriers undergo trap-assisted recombination at such interfaces which limits the electrical device performance. To reach the Shockley-Queisser power conversion efficiency (PCE) limit of 29.4%, passivating and selective contact technologies are being adopted in the silicon PV industry [3]–[5]. Generally, passivating contacts are formed by introducing an interlayer or layer stack in between the silicon surface and the metal electrode. This type of technology mitigates the inherent electrical losses in the contacted regions by suppressing charge-carrier recombination as well as maintaining a low enough resistivity [6]–[8]. The use of a well-designed passivating contact should increase the carrier collection efficiency and ultimately the PCE. Passivating both electron and hole contacts is needed in order to reach PCEs exceeding 25% [3], [9]. To date, various passivating contact structures have been successfully utilized in solar cell structures, including silicon heterojunctions (HJT) [10], poly-silicon on oxide (POLO) [11] and tunnel oxide passivated contact (TOPCon) [12], [13]. Amongst these contact architectures, a PCE of 26.81% is the best cell performance achieved so far (using HJT) [14], [15].

Typically, SiO_2 based poly-Si contacts perform better as an electron-selective contact than a hole-selective contact. The valence band offset at the SiO_2/Si interface is considerably large, resulting in a high barrier for hole tunnelling and hence a relatively low hole tunnelling current [16]. Another reason for the poorer performance as a hole-selective contact is due to the high temperature anneal step which causes dopants to diffuse from the poly-Si layer to the Si substrate. As boron diffusion in SiO_2 is not blocked as well as phosphorous, a relatively large boron concentration is found at the SiO_2/Si interface in this contact architecture which in-turn leads to Auger recombination [17]. Despite the key improvements over recent years in passivating contact technologies, the search for a hole-selective contact that can match or even exceed the performance of existing electron-selective contacts continues.

In thin film passivating contacts, the exact mechanism for charge carrier transport is still under debate in the PV community, but generally it is understood to be due to quantum tunnelling and/or through pinholes [18]–[20]. Tunnelling refers to the ability of charge carriers to have a wavefunction that can extend through a potential barrier instead of the carrier having to go over the barrier. The probability of carrier tunnelling, P_t, through such insulators is described by the Wentzel-Kramers-Brillouin (WKB) approximation [21]:

$$P_t = \exp\left(-\frac{2}{\hbar} t \sqrt{2m^* q \Delta\phi_b}\right) \qquad (1)$$

where $\hbar$ is the reduced Planck's constant, m^* is the tunnelling charge effective mass, q is the charge of an electron, t is the film thickness and $\Delta\phi_b$ is potential barrier height at the interface. From the WKB approximation, it follows that the tunnelling probability can be controlled by tuning the film thickness and potential barrier heights at the insulator/Si interface.

Utilizing thin films for carrier-selective passivating contacts requires fabrication techniques capable of attaining thicknesses with Angstrom (Å) level controllability in a reliable manner. Atomic layer deposition (ALD) offers such benefits through self-limiting surface reactions conducted at relatively low deposition temperatures. It is highly suitable for depositing a variety of materials, including oxides and nitrides, which fit the criteria for contact interlayers. Ultimately, the high level of film and interface control is highly attractive for thin film fabrication for PV applications, particularly for carrier-selective passivating contacts.

In previous work, we report the Si surface passivation quality of various types of ultrathin dielectrics grown via ALD [22]. HfO_2 was identified as the most promising candidate, with 0.9 nm of HfO_2 annealed at 450 °C providing a surface recombination velocity (SRV) of 18.6 cm s^{-1} and 2.2-3.3 nm thick HfO_2 layers achieving an SRV of ≤2.5 cm s^{-1} and J_0 of ~ 14 fA/cm^2. As the development of an efficient hole-selective contact is a key aim in today's PV industry, we determine the potential for these materials as carrier-selective interlayers. In this paper, we report an experimental study that determines the electronic barrier heights at the interface between silicon and ALD-grown Al_2O_3, HfO_2 and SiO_2. We use our existing ALD growth methods [22], [23] to grow thin films on silicon. We then use X-ray photoelectron spectroscopy (XPS) to probe the electronic core levels (CL) and valence band maximum (VBM) at the oxide/Si interface. Additionally, we use simulations in Sentaurus TCAD [24] to estimate the contact resistivity that we would expect in a Si/oxide/poly-Si p-contact formation for each of the investigated oxides. Since the barrier tunnelling model in Sentaurus is based on the WKB approximation (1), the resulting contact resistivities highly depend on the oxide thickness, t, as well as the effective (hole) tunnelling mass, m_h^*. Assuming hole tunneling masses from literature, these simulations indicate that reasonable contact properties could be achieved and therefore provide an incentive for further experimental research on the development of an efficient hole-selective contact based on these oxides. Beyond minimizing contact resistivity, the use of these dielectrics as interlayers in carrier-selective passivating contacts requires the enhancement of the surface passivation properties of these films at ultra-thin (sub-3 nm) thicknesses, as explored in Ref. [22].

II. Experimental Methods

A. Specimen Fabrication

ALD films were grown on *p*-type (gallium doped) Si (Cz, 5 Ω cm, <100>, 125 μm thick) substrates that were prepared following a previously reported chemical cleaning and etching procedure [22], [25]. In the first ALD half-cycle reaction, trimethylaluminum, tetrakis(dimethylamido)hafnium and bis(diethylamido)silane precursors were used to grow Al_2O_3, HfO_2 and SiO_2 films, respectively. An O_2 plasma source was used for the second half-cycle reaction for all three films. All films were grown at a deposition temperature of 200 °C. Growth rates per cycle are reported as 1.3 Å/cycle (Al_2O_3), 1 Å/cycle (HfO_2) and 0.6 Å/cycle (SiO_2) [26], and re-evaluated in [22]. A post-deposition anneal was conducted at 450 °C for 30 minutes for Al_2O_3 and HfO_2, and 800 °C for 30 minutes for SiO_2. All films were grown in a Veeco Fiji G2 plasma-enhanced ALD chamber.

B. X-ray Photoelectron Spectroscopy

XPS was conducted using a Kratos Axis Ultra DLD spectrometer. For XPS, all samples were mounted on a non-magnetic, stainless-steel bar by using electrically conductive carbon tape. XPS was conducted using a monochromated Al Kα X-ray (1.487 keV) source. The energy resolution of the detector was 0.4 eV. Measurements were conducted at room temperature and at a take-off angle of 90° with respect to the sample surface. The CL spectra and the VBMs were measured using a pass energy of 20 eV, all from an analysis area of 300 μm × 700 μm. To avoid charging effects, a charge neutraliser gun was used for all XPS measurements. Fitting procedures to extract peak positions and relative stoichiometries were performed by using the Casa XPS software. These were fitted and corrected using their corresponding sensitivity factors, taking the mean free path of the photoelectrons and photoionization cross sections of these core levels into account.

C. Electronic Band Offsets Determination

Determination of the valence band offset (ΔE_V) and conduction band offset (ΔE_C) at a semiconductor interface can be done using Kraut's method [27]–[31]. These are depicted in the schematic diagram of the band offsets in Fig. 1.

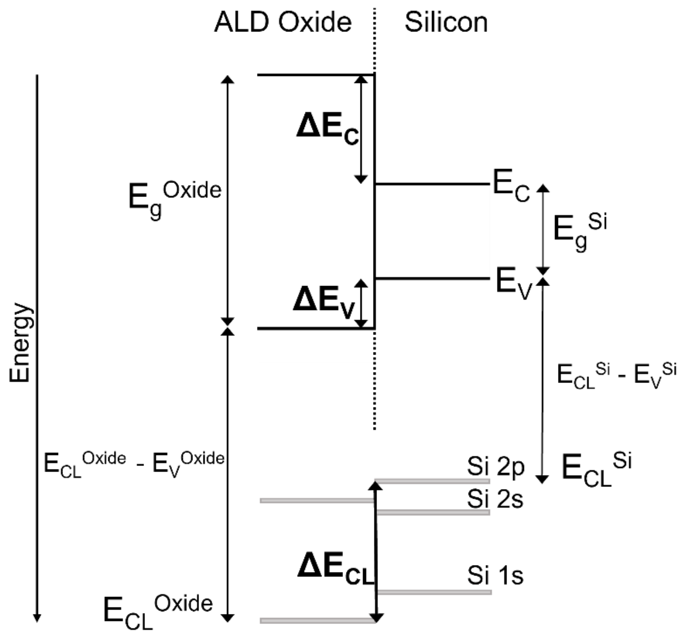

Fig. 1. Schematic diagram of band offsets at an oxide/Si interface.

This X-ray photoemission-based method uses Poisson's equation to predict the band discontinuities based on the deviations in charge distribution found at the interface relative to the semiconductor bulk. In this approach, the position of the core level at the interface, as well as the binding energy difference between the semiconductor CL and the VBM are required to determine the valence band offset:

$$\Delta E_v = \left(E_{CL}^{Si} - E_{CL}^{Oxide}\right)_{Oxide/Si} - \left(E_{CL}^{Si} - E_V^{Si}\right)_{Si} + \left(E_{CL}^{Oxide} - E_V^{Oxide}\right)_{Oxide} \quad (2)$$

In this equation, $(E_{CL}^{Si} - E_{CL}^{Oxide})_{Oxide/Si}$ is the energy difference between the CL of the two materials at the interface, namely ΔE_{CL}. Based on the XPS photoelectron sampling depth being under 5 nm in these ALD-grown materials [32], [33], 2 nm and 3 nm thick films on Si were used to obtain two sets of measurements that probe the interface. To complete the equation for ΔE_V, the energy difference between the CL centroids and VBM for Si and all the ALD oxides of interest were obtained from XPS of the respective thick films. For this experiment, the Al 2p, Hf 4f and Si 2p orbital peaks were used as the CL for Al_2O_3, HfO_2 and SiO_2, respectively. The elemental silicon region of the Si 2p peak was also used as the CL for Si. For E_V^{Si} and E_V^{Oxide} determination, linear extrapolation of the leading edge to the baseline of the valence band spectra from the respective thick films were used.

Once ΔE_V was determined, ΔE_C was calculated following Kraut's method [27]:

$$\Delta E_C = \Delta E_V - \left(\Delta E_g\right)_{Si/Oxide} \quad (3)$$

where $(\Delta E_g)_{Si/Oxide}$ is the energy difference between the band gap of Si and the respective ALD oxide films. An optical band gap of 1.12 ± 0.01 eV was used for E_g^{Si} in these calculations.

III. Results and Discussion

A. Electronic Band Offsets

The electronic band offsets at a Al_2O_3/Si, HfO_2/Si and SiO_2/Si interface have been reported in the literature. A summary of these calculations from previous reports is presented in Table I.

TABLE I
REPORTED VALENCE BAND OFFSET (ΔE_V) AND CONDUCTION BAND OFFSET (ΔE_C) FOR Al_2O_3/Si, HfO_2/Si AND SiO_2/Si TAKEN FROM LITERATURE.

Al_2O_3/Si		**HfO_2/Si**		**SiO_2/Si**	
ΔE_V (eV)	ΔE_C (eV)	ΔE_V (eV)	ΔE_C (eV)	ΔE_V (eV)	ΔE_C (eV)
4.9 [34]	2.8 [34]	3.4 [34]	1.5 [34]	4.54 [16]	3.15 [16]
4.1 [35]	3.5 [35]	2.87 [36]	1.71 [36]	4.49 [37]	3.29 [37]
3.5 [38]	-	2.69 [39]	2.0 [39]	4.4 [34]	3.5 [34]
3.24 [36]	2.44 [36]	2.5 [40]	2.2 [40]	4.3 [38]	-
2.95 [41]	2.1 [41]	2.5 [42]	2.0 [42]	-	3.13 [43]
-	2.13 [44]				

A large range of band offsets have been presented over the last couple of decades. For example, ΔE_V at a Al_2O_3/Si interface has been reported between 2.95 eV and 4.9 eV. The differences are mainly due to dissimilarities in fabrication processes that result in variations in chemical composition and stoichiometry that in turn lead to alterations in the band offsets. For example, Alay *et al.* suggest differences in the band offsets for SiO_2/Si based on whether the SiO_2 layer was fabricated by a dry or wet chemical process as well as the crystal orientation of the underlying Si substrate being (100) or (111) [37]. Interfacial effects such as interfacial dipoles could also lead to deviations in band offsets. For ΔE_{CL} determination (as part of (2)), the thickness of the overlayer chosen can also play a role in the band offset calculations. It is generally understood that the thickness must not exceed the photoelectron sampling depth of the overlaying material, but variations in thickness below that limit can cause small shifts in the CL positions. Also, differences in measurement procedures (*e.g.*, XPS, linear internal photoemission, and synchrotron radiation photoemission) add further uncertainty in the reported band offsets. To accurately determine the probability of carrier tunnelling through such interfaces, precise determination of the band offsets is required.

Using XPS, we have identified the core level energy centroids and valence band edges for Si, Al_2O_3, HfO_2 and SiO_2, as shown in Fig. 2. From Fig. 2 (a) and 2 (b), the Si 2p CL energy and leading edge of the valence band spectra (i.e. VBM) for bare (native oxide stripped with HF) Si are determined to be 99.71 ± 0.02 eV and 0.69 ± 0.04 eV, respectively. The ± symbol is used to signify the measurement uncertainty. Hence, $(E_{CL}^{Si} - E_V^{Si})_{Si}$ is calculated to be 99.02 ± 0.045 eV. The propagated uncertainty is determined as the square root of the sum of the

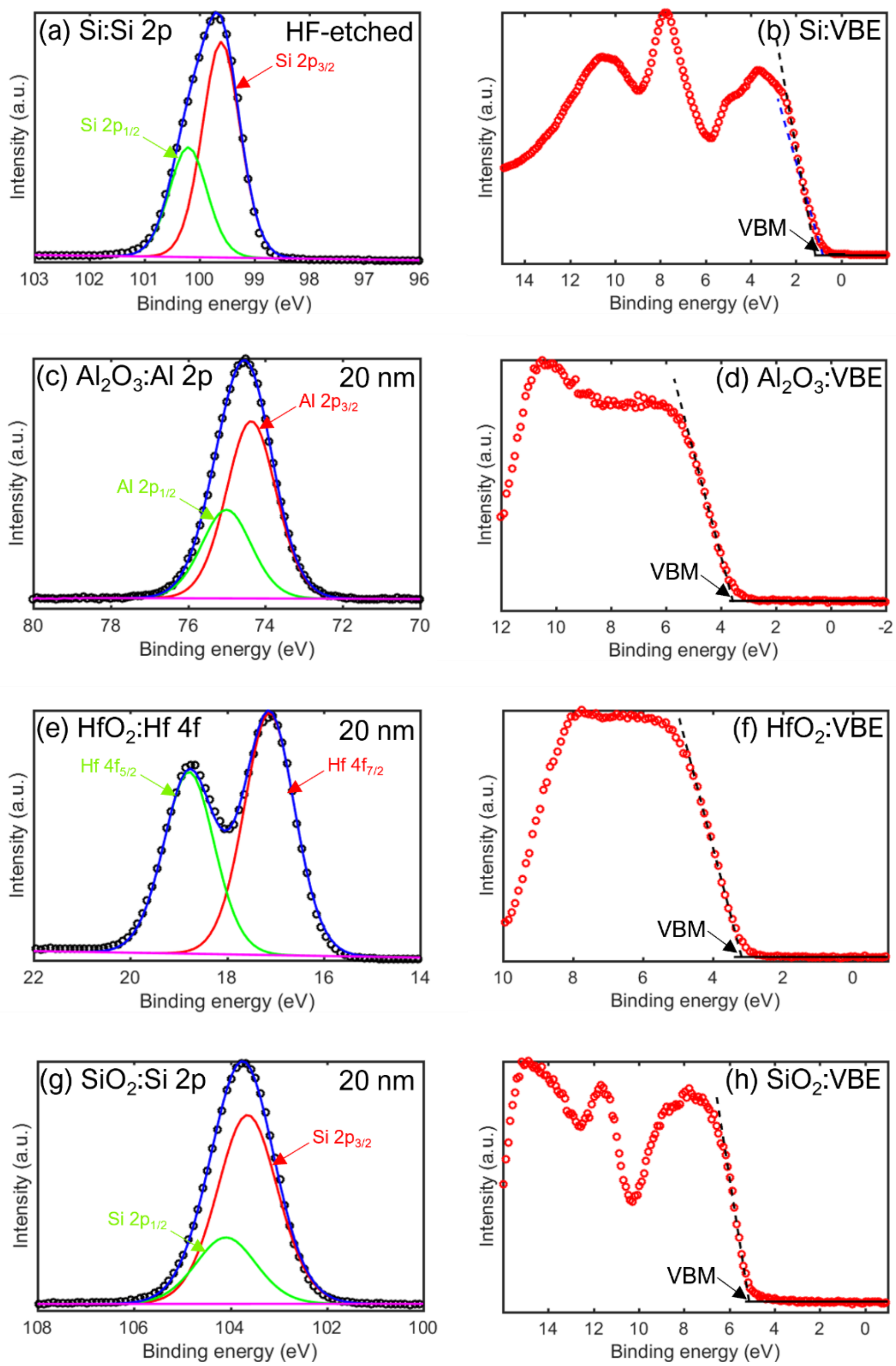

Fig. 2. XPS spectra showing: (a) Si 2p CL and (b) VBM for bulk *p*-type Si, (c) Al 2p CL and (d) VBM for bulk Al_2O_3, (e) Hf 4f CL and (f) VBM from bulk HfO_2 and (g) Si 2p CL and (h) VBM for bulk SiO_2. Circle symbols denote measurements, solid lines denote fitted subcomponents and their superposition and dashed lines illustrate the extraction of the VBM.

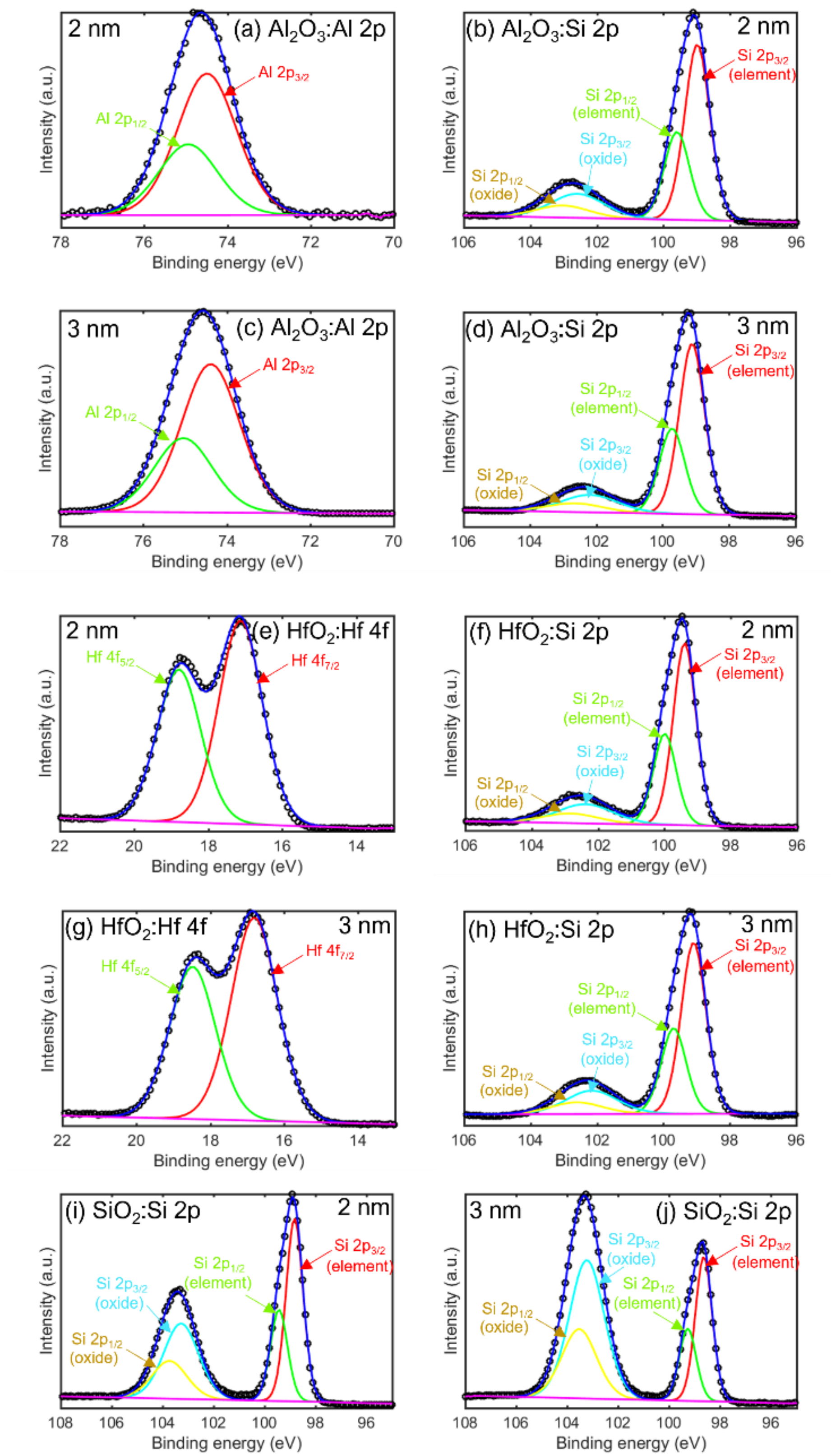

Fig. 3. XPS spectra showing (a) Al 2p CL and (b) Si 2p CL from 2 nm Al_2O_3 on Si, (c) Al 2p CL and (d) Si 2p CL from 3 nm Al_2O_3 on Si, (e) Hf 4f CL and (f) Si 2p CL from 2 nm HfO_2 on Si, (g) Hf 4f CL and (h) Si 2p CL from 3 nm HfO_2 on Si, (i) Si 2p CL from 2 nm SiO_2 on Si and (j) Si 2p CL from 3 nm SiO_2 on Si. Circle symbols denote measurements, solid lines denote fitted subcomponents and their superposition.

squares of E_{CL} and E_V. Fig. 2 (c) and 2 (d) show the Al 2p CL energy and VBM for Al_2O_3. The Al 2p CL is determined at a binding energy of 74.50 ± 0.02 eV and the VBM at 3.37 ± 0.04 eV. From this, $(E_{CL}^{Al2O3} - E_V^{Al2O3})_{Al2O3}$ is calculated to be 71.13 ± 0.045 eV. For bulk HfO_2, the Hf 4f CL energy and VBM, shown in Fig. 2 (e) and 2 (f), are determined as 17.12 ± 0.02 eV and 3.15 ± 0.04 eV, respectively. Hence, $(E_{CL}^{HfO2} - E_V^{HfO2})_{HfO2}$ is calculated to be 13.97 ± 0.045 eV. From Fig. 2 (g) and 2 (h), the Si 2p CL energy and VBM for SiO_2 are determined as 103.68 ± 0.02 eV and 5.02 ± 0.04 eV, respectively. Therefore, $(E_{CL}^{SiO2} - E_V^{SiO2})_{SiO2}$ is calculated to be 98.66 ± 0.045 eV. A summary of the XPS data taken from Fig. 2 can be found in Table II.

TABLE II
PARAMETERS EXTRACTED FROM THE XPS DATA SHOWN IN FIG. 2 FOR ΔE_V CALCULATIONS.

Bulk material	E_{CL} (eV)	E_V (eV)	$(E_{CL}-E_V)$ (eV)
Silicon	99.71 ± 0.02	0.69 ± 0.04	99.02 ± 0.045
Al_2O_3	74.50 ± 0.02	3.37 ± 0.04	71.13 ± 0.045
HfO_2	17.12 ± 0.02	3.15 ± 0.04	13.97 ± 0.045
SiO_2	103.68 ± 0.02	5.02 ± 0.04	98.66 ± 0.045

The CL for Al_2O_3 (Al 2p) and Si (Si 2p) at the interface from the 2 nm and 3 nm thick Al_2O_3 specimens are shown in Fig. 3 (a)-(d). From Fig. 3 (b) and 3 (d), two peaks are seen for the Si 2p CL at the interface. The CL found at ~99 eV is detected from elemental silicon and the CL at ~103 eV is from the presence of SiO_2. This CL verifies the presence of SiO_2 in these specimens, suggesting the manifestation of a very thin SiO_2 layer at the Al_2O_3/Si interface [45]. For this study, we focus on only using the elemental silicon region for E_{CL}^{Si} in the band offset calculations.

From Fig. 3 (a) and 3 (c), the Al 2p CL from 2 nm and 3 nm thick Al_2O_3 on Si are found at binding energies of 74.62 ± 0.02 eV and 74.55 ± 0.02 eV, respectively. Additionally, Fig. 3 (b) and 3 (d) show the Si 2p CL, with the binding energies found at 99.12 ± 0.02 eV and 99.25 ± 0.02 eV. Hence, $(E_{CL}^{Si} - E_{CL}^{Al2O3})_{Al2O3/Si}$ is determined for the 2 nm and 3 nm Al_2O_3 specimen as 24.50 ± 0.028 eV and 24.70 ± 0.028 eV, respectively.

Fig. 3 (e)-(h) show the Hf 4f and Si 2p CL from 2 nm and 3 nm thick HfO_2 on Si. From Fig. 3 (e) and 3 (g), the Hf 4f CL binding energies are determined as 17.13 ± 0.02 eV and 16.81 ± 0.02 eV. The Si 2p CL in Fig. 3 (f) and 3 (h) show a peak at ~103 eV as well as the Si 2p elemental silicon peak at ~99 eV, which again demonstrates the presence of an interfacial SiO_2 layer. Taking the elemental silicon contribution into account, the Si 2p CL for 2 nm and 3 nm thick HfO_2 on Si are found at 99.46 ± 0.02 eV and 99.23 ± 0.02 eV, respectively. Therefore, $(E_{CL}^{Si} - E_{CL}^{HfO2})_{HfO2/Si}$ for 2 nm and 3 nm thick HfO_2 on Si are determined to be 82.33 ± 0.028 eV and 82.42 ± 0.028 eV, respectively.

Fig. 3 (i) and 3 (j) show the Si 2p CL peaks from 2 nm and 3 nm thick SiO_2 on Si, respectively. Here, we only take the Si 2p into account as we detect contributions from elemental Si and Si-O in the same binding energy region. From Fig. 3 (i) and 3 (j), the Si 2p (Si-O) CL peaks are found at binding energies of 103.28 ± 0.02 eV and 103.23 ± 0.02 eV. Si 2p (elemental) peaks are detected at binding energies of 98.83 ± 0.02 eV and 98.65 ± 0.02 eV. Hence, for 2 nm and 3 nm thick SiO_2 on Si, $(E_{CL}^{Si} - E_{CL}^{SiO2})_{SiO2}$ are calculated to be -4.45 ± 0.028 eV and -4.58 ± 0.028 eV, respectively. A summary of the XPS data and corresponding calculations taken from Fig. 3 are shown in Table III.

TABLE III
XPS DATA TAKEN FROM FIG. 2 AND 3 FOR ΔE_V CALCULATIONS.

Interface	E_{CL}^{Si}	E_{CL}^{Oxide}	E_{CL}^{Si} - E_{CL}^{Oxide}
(2nm)Al_2O_3/Si	99.12 ± 0.02	74.62 ± 0.02	24.50 ± 0.028
(3nm)Al_2O_3/Si	99.25 ± 0.02	74.55 ± 0.02	24.70 ± 0.028
(2 nm)HfO_2/Si	99.46 ± 0.02	17.13 ± 0.02	82.33 ± 0.028
(3 nm)HfO_2/Si	99.23 ± 0.02	16.81 ± 0.02	82.42 ± 0.028
(2 nm)SiO_2/Si	98.83 ± 0.02	103.28 ± 0.02	-4.45 ± 0.028
(3 nm)SiO_2/Si	98.65 ± 0.02	103.23 ± 0.02	-4.58 ± 0.028

From Tables II and III, ΔE_V and ΔE_C are calculated using (2) and (3) respectively and are shown in Table IV. To determine ΔE_C, we use a bandgap of 6.65 ± 0.11 eV for Al_2O_3 [46], 5.6 ± 0.2 eV for HfO_2 [47], [48] and 8.6 ± 0.1 eV for SiO_2 [49]. For $(E_{CL}^{Si} - E_{CL}^{Oxide})_{Oxide/Si}$ in (2), an average is taken between the 2 nm and 3 nm oxide/Si calculations from Table III. From these results, Fig. 4 shows a simplified schematic diagram of the band offsets at the Al_2O_3/Si, HfO_2/Si and SiO_2/Si interface.

TABLE IV
CALCULATED VALENCE AND CONDUCTION BAND OFFSETS.

Interface	ΔE_V (eV)	ΔE_C (eV)
Al_2O_3/Si	3.29 ± 0.07	2.24 ± 0.13
HfO_2/Si	2.67 ± 0.07	1.81 ± 0.21
SiO_2/Si	4.87 ± 0.07	2.61 ± 0.12

The $\Delta E_C/\Delta E_V$ ratio is a good indication of favorability towards electron/hole transport, where $\Delta E_C/\Delta E_V > 1$ favors hole transport. For Al_2O_3/Si, HfO_2/Si and SiO_2/Si, $\Delta E_C/\Delta E_V$ can be determined as 0.68, 0.68 and 0.54, respectively. This suggests that all three interfaces would favor electron transport, with SiO_2 being the most favorable towards electrons. SiO_2 is used as the passivating interlayer in the world-leading carrier-selective passivating contact technology, TOPCon, and is known to perform far better as an electron contact than as a hole contact [3]. The band offsets determined indicate that HfO_2 and Al_2O_3 could offer alternatives for SiO_2 in the hole-selective counterpart. Beyond $\Delta E_C/\Delta E_V$, a direct comparison of the absolute values for ΔE_V determined for the three oxides of interest is another good indication towards hole transport favorability (based on (1)). Evidently, HfO_2 possesses the smallest potential barrier for hole transport but a ΔE_V of 2.67 eV is still considerably large.

The band offsets are not the only figure of merit when considering fitting candidates for carrier-selective contacts so

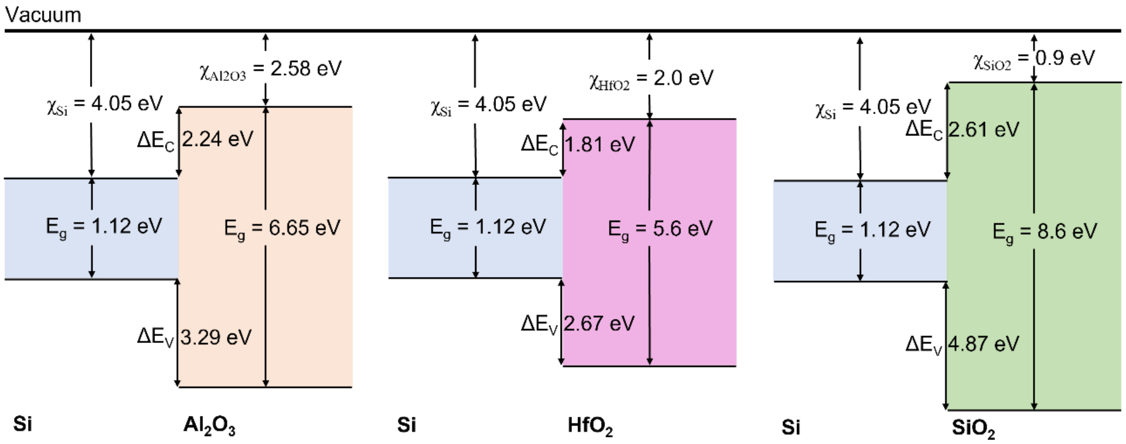

Fig. 4. Simplified schematic diagram of measured conduction band offset and valence band offsets of ALD-deposited Al_2O_3, HfO_2 and SiO_2 on Si.

the impact of this must be weighed with their suitability in other important factors, including carrier tunnelling mass and surface recombination velocity. We explored the Si surface passivation quality in previous work [22] and determine the impact of the band offsets and tunnelling masses on the contact resistivity using TCAD simulations here.

B. Contact Resistivity Estimation via TCAD Simulations

For charge carrier transport through ultrathin dielectrics, one of the theories that is strongly agreed upon is quantum tunnelling through the potential barrier created at the Si surface. Based on the WKB approximation (1), the tunnelling probability is dependent on the barrier height and film thickness, as well as the effective tunnelling masses of the charge carriers.

Using the barrier heights determined for the ALD oxides with respect to Si, Sentaurus TCAD is used to estimate the contact resistivity for a range of thicknesses in a typical p-TOPCon format. The contact resistivity is extracted directly from the TCAD simulations for this study, An illustration of the contact structure (i.e. poly-Si/oxide/Si) we are interested in is shown in Fig. 5 (a). A *p*-type Si (1 Ω cm, 200 µm thick) substrate with the ALD oxides on the front side was devised, with a 50 nm thick p^+ poly-Si conductive interlayer (with 10^{20} cm^{-3} doping concentration) between the metal contact and the oxide. In the TCAD simulations, an electron effective mass of 0.25 m_0 [46], a hole effective mass of 0.36 m_0 [50] and an optical bandgap of 6.65 eV [46] were used for Al_2O_3, where m_0 is the free electron mass. For HfO_2, an electron effective mass of 0.11 m_0 [51], a hole effective mass of 0.58 m_0 [51], [52] and an optical bandgap of 5.6 eV [47], [48] were used as taken from literature. For SiO_2, an electron effective mass of 0.4 m_0 [53], [54], a hole effective mass of 0.3 m_0 [55] and an optical bandgap of 8.6 eV were used. Fig. 5(b) shows the tunnelling layer thickness vs. calculated contact resistivity (ρ_c) for ALD-grown Al_2O_3, HfO_2, and SiO_2 on p-Si as a hole-selective contact.

The calculated ρ_c vs dielectric thickness curves show an exponential trend in all three cases. The difference in ρ_c between the three ALD-grown dielectrics below 1.1 nm is negligible. From Fig. 5(b), the Al_2O_3/(p)Si based contact outperforms HfO_2 and SiO_2 (i.e., the lowest ρ_c) at most thicknesses. Despite the larger ΔE_V measured for Al_2O_3/Si in comparison to HfO_2/Si, the Al_2O_3/Si contact outperforms HfO_2/Si due to the considerably lower hole effective mass. This demonstrates how crucially the contact resistivity depends on the assumed tunnelling masses. Based on (1), the tunnelling effective mass and interfacial barrier heights are of equal importance and ideally, both parameters should be low enough to ensure a low contact resistivity.

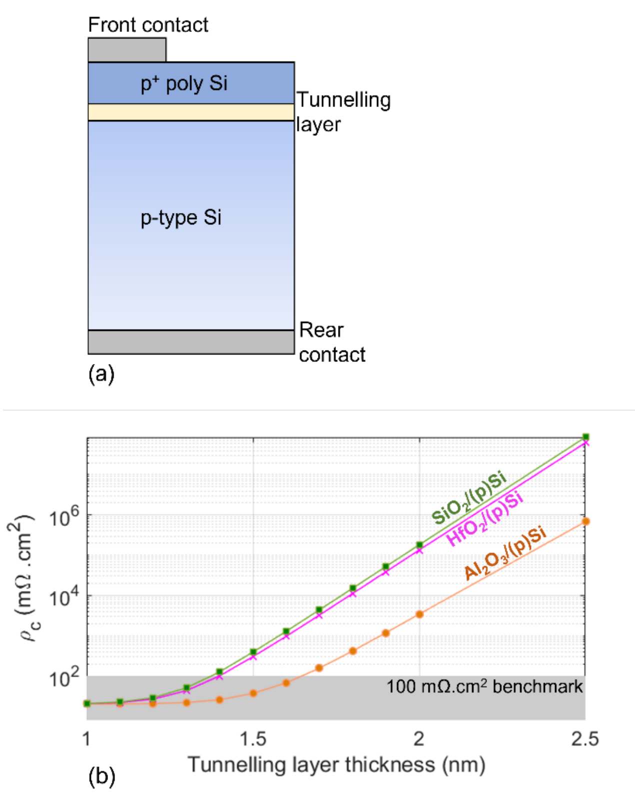

Fig. 5. (a) Schematic of structure simulated via TCAD and (b) tunnelling layer thickness vs contact resistivity for ALD-grown Al_2O_3, HfO_2 and SiO_2 on *p*-type Si.

As a standard for carrier-selective passivating contacts, a contact resistivity of 100 mΩ.cm^2 is seen as the upper threshold for high-performance full-area contacts. Achieving a contact resistivity below 100 mΩ.cm^2 provides insignificant improvements to the fill factor, and hence the PCE of such devices. Based on our TCAD simulations with the given effective tunnelling masses from literature, a thickness of 1.65 nm is found as the upper limit for Al_2O_3. The upper limit for both HfO_2 and SiO_2 is determined as 1.4 nm.

Incorporating metal oxides like Al_2O_3 with poly-Si for hole-selective passivating contacts have seen some success in literature, with the contact resistivity reported at 200 mΩ.cm^2 in multiple findings in literature [56]–[58]. This further illuminates the scope for research on Al_2O_3-based hole-selective passivating contacts. For HfO_2, despite showing a higher contact resistivity than Al_2O_3 in our TCAD simulations, the surface recombination velocities determined for ultrathin HfO_2 layers outperform Al_2O_3, operating just as well as thicker HfO_2 films [59], as found in our previous work[22], [60]. These results were achieved without common post-deposition treatments like hydrogenation, which are typically used to enhance the surface passivation properties [22], [57], [61]. However, the impact of growing a p$^+$ poly-Si layer on the oxides as well as annealing for crystallizing the poly-Si layer at temperatures exceeding 800 ºC is yet to be examined. Also, the use of ALD-grown SiO_2 as a replacement for thermally grown SiO_2 still requires substantial improvements, mainly due to the inferior passivation quality of this type of SiO_2 growth method [13], [22], [57].

IV. Conclusion

We explored the electronic band offsets of ALD-grown Al_2O_3, HfO_2 and SiO_2 on silicon using a photoemission-based method. For Al_2O_3/Si, we determine ΔE_V and ΔE_C as 3.29 ± 0.07 eV and 2.24 ± 0.13 eV, respectively. For HfO_2/Si, ΔE_V and ΔE_C are determined as 2.67 ± 0.07 eV and 1.81 ± 0.21 eV, whilst for SiO_2/Si ΔE_V and ΔE_C are 4.87 ± 0.07 eV and 2.61 ± 0.12 eV, respectively. We apply TCAD simulations to predict the contact resistivity at various dielectric thicknesses with a 50 nm p$^+$ polycrystalline silicon conductive layer between the metal electrode and thin dielectrics and assuming hole effective tunnelling masses taken from literature. In order to form an efficient hole-selective contact with a p-type polysilicon electrode and to not exceed the 100 mΩ.cm^2 contact resistivity benchmark, an upper limit of 1.65 nm in thickness is determined for Al_2O_3, whilst 1.4 nm is calculated as the threshold for HfO_2 and SiO_2. Experimental demonstration of the contact resistivity for such structures will be part of future work.

Data Access Statement

Data underpinning figures in this paper can be downloaded from https://wrap.warwick.ac.uk/75494. Requests for additional data should be made directly to the corresponding author.

References

[1] IEA, "IEA - Data & Statistics," Dec 2022. [Online] Available: https://www.iea.org/subscribe-to-data-services/electricity-statistics

[2] B. Min, M. Müller, H. Wagner, G. Fischer, R. Brendel, P. P. Altermatt, and H. Neuhaus, "A Roadmap Toward 24% Efficient PERC Solar Cells in Industrial Mass Production," *IEEE J. Photovoltaics*, vol. 7, no. 6, pp. 1541–1550, 2017, doi: 10.1109/JPHOTOV.2017.2749007.

[3] T. Allen, J. Bullock, X. Yang, A. Javey, and S. De Wolf, "Passivating contacts for crystalline silicon solar cells," *Nat. Energy*, vol. 4, pp. 914–928, 2019, doi: 10.1038/s41560-019-0463-6.

[4] T. Niewelt, B. Steinhauser, A. Richter, B. Veith-Wolf, A. Fell, B. Hammann, N. E. Grant, L. Black, J. Tan, A. Youssef, J. D. Murphy, J. Schmidt, M. C. Schubert, and S. W. Glunz, "Reassessment of the intrinsic bulk recombination in crystalline silicon," *Sol. Energy Mater. Sol. Cells*, vol. 235, p. 111467, 2022, doi: 10.1016/j.solmat.2021.111467.

[5] K. Masuko, M. Shigematsu, T. Hashiguchi, D. Fujishima, M. Kai, N. Yoshimura, T. Yamaguchi, Y. Ichihashi, T. Mishima, N. Matsubara, T. Yamanishi, T. Takahama, M. Taguchi, E. Maruyama, and S. Okamoto, "Achievement of More Than 25% Conversion Efficiency With Crystalline Silicon Heterojunction Solar Cell," *IEEE J. Photovoltaics*, vol. 4, no. 6, pp. 1433–1435, 2014, doi: 10.1109/JPHOTOV.2014.2352151.

[6] J. Melskens, B. W. H. Van De Loo, B. Macco, L. E. Black, S. Smit, and W. M. M. E. Kessels, "Passivating Contacts for Crystalline Silicon Solar Cells : From Concepts and Materials to Prospects," *IEEE J. Photovoltaics*, vol. 8, no. 2, pp. 373–388, 2018, doi: 10.1109/JPHOTOV.2018.2797106.

[7] Z. Wang, P. Li, Z. Liu, J. Fan, X. Qian, J. He, S. Peng, D. He, M. Li, and P. Gao, "Hole selective materials and device structures of heterojunction solar cells : Recent assessment and future trends Hole selective materials and device structures of heterojunction solar cells : Recent assessment and future trends," *APL Mater.*, vol. 7, no. 11, p. 110701, 2019, doi: 10.1063/1.5121327.

[8] E. Khorani, S. McNab, T. E. Scheul, T. Rahman, R. S. Bonilla, S. A. Boden, and P. R. Wilshaw, "Optoelectronic properties of ultrathin ALD silicon nitride and its potential as a hole-selective nanolayer for high efficiency solar cells," *APL Mater.*, vol. 8, no. 11, p. 111106, 2020, doi: 10.1063/5.0023336.

[9] R. Brendel and R. Peibst, "Contact Selectivity and Efficiency in Crystalline Silicon Photovoltaics," *IEEE J. Photovoltaics*, vol. 6, no. 6, pp. 1413–1420, 2016, doi: 10.1109/JPHOTOV.2016.2598267.

[10] X. Yang and K. Weber, "N-type silicon solar cells featuring an electron-selective TiO_2 contact," *2015 IEEE 42nd Photovolt. Spec. Conf. PVSC 2015*, pp. 37–40, 2015, doi: 10.1109/PVSC.2015.7356139.

[11] C. Hollemann, F. Haase, S. Schäfer, J. Krügener, R. Brendel, and R. Peibst, "26.1%-efficient POLO-IBC cells: Quantification of electrical and optical loss mechanisms," *Prog. Photovoltaics Res. Appl.*, vol. 27, no. 11, pp. 950–958, 2019, doi: 10.1002/pip.3098.

[12] F. Feldmann, M. Simon, M. Bivour, C. Reichel, M. Hermle, and S. W. Glunz, "Carrier-selective contacts for Si solar cells," *Appl. Phys. Lett.*, vol. 104, no. 181105, 2014, doi: 10.1063/1.4875904.

[13] F. Feldmann, M. Bivour, C. Reichel, H. Steinkemper, M. Hermle, and S. W. Glunz, "Tunnel oxide passivated contacts as an alternative to partial rear contacts," *Sol. Energy Mater. Sol. Cells*, vol. 131, pp. 46–50, 2014, doi: 10.1016/j.solmat.2014.06.015.

[14] LONGi, "At 26.81%, LONGi sets a new world record efficiency for silicon solar cells," Nov 2022. [Online] Available: https://www.longi.com/en/news/propelling-the-transformation/

[15] M. A. Green, E. D. Dunlop, J. Hohl-Ebinger, M. Yoshita, N. Kopidakis, and X. Hao, "Solar cell efficiency tables," *Prog. Photovoltaics Res. Appl.*, vol. 30, no. 1, pp. 3–12, 2022, doi: 10.1002/pip.3506.

[16] E. Bersch, S. Rangan, R. A. Bartynski, E. Garfunkel, and E. Vescovo, "Band offsets of ultrathin high- κ oxide films with Si," *Phys. Rev. B 78 - Condens. Matter Mater. Phys.*, vol. 78, no. 8, p. 085114, 2008, doi: 10.1103/PhysRevB.78.085114.

[17] F. Feldmann, J. Schön, J. Niess, W. Lerch, and M. Hermle, "Studying dopant diffusion from Poly-Si passivating contacts," *Sol. Energy Mater. Sol. Cells*, vol. 200, p. 109978, 2019, doi: 10.1016/j.solmat.2019.109978.

[18] A. Campa, F. Smole, N. Folchert, T. Wietler, B. Min, R. Brendel, and

M. Topic, “Detailed Analysis and Understanding of the Transport Mechanism of Poly-Si-Based Carrier Selective Junctions,” *IEEE J. Photovoltaics*, vol. 9, no. 6, pp. 1575–1582, Nov. 2019, doi: 10.1109/JPHOTOV.2019.2943610.

[19] A. S. Kale, W. Nemeth, S. U. Nanayakkara, H. Guthrey, M. Page, M. Al-Jassim, S. Agarwal, and P. Stradins, “Tunneling or Pinholes: Understanding the Transport Mechanisms in SiO_x Based Passivated Contacts for High-Efficiency Silicon Solar Cells,” in *2018 IEEE 7th World Conference on Photovoltaic Energy Conversion, WCPEC 2018 - A Joint Conference of 45th IEEE PVSC, 28th PVSEC and 34th EU PVSEC*, Nov. 2018, pp. 3473–3476. doi: 10.1109/PVSC.2018.8547211.

[20] Y. Liu, P. Stradins, H. Deng, J. Luo, and S. H. Wei, “Suppress carrier recombination by introducing defects: The case of Si solar cell,” *Appl. Phys. Lett.*, vol. 108, no. 2, p. 022101, Jan. 2016, doi: 10.1063/1.4939628.

[21] H. C. De Graaff and J. G. De Groot, “The SIS Tunnel Emitter: A Theory for Emitters with Thin Interface Layers,” *IEEE Trans. Electron Devices*, vol. 26, no. 11, pp. 1771–1776, 1979, doi: 10.1109/T-ED.1979.19684.

[22] S. L. Pain, E. Khorani, T. Niewelt, A. Wratten, G. J. P. Fajardo, B. P. Winfield, R. S. Bonilla, M. Walker, L. F. J. Piper, N. E. Grant, and J. D. Murphy, “Electronic Characteristics of Ultra-Thin Passivation Layers for Silicon Photovoltaics,” vol. 9, p. 2201339, 2022, doi: 10.1002/admi.202201339.

[23] J. D. Murphy, N. E. Grant, S. L. Pain, T. Niewelt, A. Wratten, E. Khorani, V. P. Markevich, A. R. Peaker, P. P. Altermatt, J. S. Lord, and K. Yokoyama, “Carrier lifetimes in high-lifetime silicon wafers and solar cells measured by photoexcited muon spin spectroscopy,” *J. Appl. Phys.*, vol. 132, no. 065704, 2022, doi: 10.1063/5.0099492.

[24] Synopsys, “Sentaurus Device User Guide: release Q-2019.12,” 2019. [Online] Available: https://www.synopsys.com/silicon/tcad/device-simulation/sentaurus-device.html

[25] N. E. Grant, P. P. Altermatt, T. Niewelt, R. Post, W. Kwapil, M. C. Schubert, and J. D. Murphy, “Gallium-Doped Silicon for High-Efficiency Commercial Passivated Emitter and Rear Solar Cells,” *Sol. RRL*, vol. 5, no. 4, p. 2000754, 2021, doi: 10.1002/solr.202000754.

[26] “Veeco Data Sheets,” June 2018. [Online] Available: https://www.gammadata.se/assets/Uploads/Fiji-G2-product-sheet-2018.pdf

[27] E. A. Kraut, R.W. Grant, J.R. Waldrop, and S.P. Kowalczyk, “Precise Determination of the Valence-Band Edge in X Ray Photoemission Spectra,” *Phys. Rev. Lett.*, vol. 44, no. 24, p. 1620, 1980, doi: 10.1103/PhysRevLett.44.1620.

[28] E. A. Kraut, R. W. Grant, J. R. Waldrop, and S. P. Kowalczyk, “Semiconductor core-level to valence-band maximum binding-energy differences: Precise determination by x-ray photoelectron spectroscopy,” *Phys. Rev. B*, vol. 28, no. 4, pp. 1965–1977, 1983, doi: 10.1103/PhysRevB.28.1965.

[29] S. A. Chambers, “Band discontinuities at epitaxial $SrTiO_3$/Si(001) heterojunctions,” *Appl. Phys. Lett.*, vol. 77, no. 11, pp. 1662–1664, 2000, doi: 10.1063/1.1310209.

[30] X. Lou, X. Gong, J. Feng, and R. Gordon, “Band-Offset Analysis of Atomic Layer Deposition La_2O_3 on GaAs(111), (110), and (100) Surfaces for Epitaxial Growth,” *ACS Appl. Mater. Interfaces*, vol. 11, no. 31, pp. 28515–28519, 2019, doi: 10.1021/acsami.9b08436.

[31] T. Zhang, M. A. Hossain, C. Y. Lee, Y. Zakaria, A. A. Abdallah, and B. Hoex, “Atomic layer deposited $Zn_xNi_{1-x}O$: A thermally stable hole selective contact for silicon solar cells,” *Appl. Phys. Lett.*, vol. 113, no. 26, 2018, doi: 10.1063/1.5056223.

[32] S. Tougaard, “QUASES-IMFP-TPP2MM,” 2016. [Online] Available: http://www.quases.com/products/quases-imfp-tpp2m/

[33] S. Tanuma, C. Powell, and D. Penn, “Calculations of electron inelastic mean free paths. V. Data for 14 organic compounds over the 50–2000 eV range,” *Surf. Interface Anal.*, vol. 21, pp. 165–176, 1994.

[34] J. Robertson, “Band offsets of wide-band-gap oxides and implications for future electronic devices,” *J. Vac. Sci. Technol. B Microelectron. Nanom. Struct.*, vol. 18, no. 3, pp. 1785–1791, 2000, doi: 10.1116/1.591472.

[35] R. Yan, Q. Zhang, O. A. Kirillov, W. Li, J. Basham, A. Boosalis, X. Liang, D. Jena, C. A. Richter, A. C. Seabaugh, D. J. Gundlach, H. G. Xing, and N. V. Nguyen, “Graphene as transparent electrode for direct observation of hole photoemission from silicon to oxide,” *Appl. Phys. Lett.*, vol. 102, p. 123106, 2013, doi: 10.1063/1.4796169.

[36] H. L. Lu, M. Yang, Z. Y. Xie, Y. Geng, Y. Zhang, P. F. Wang, Q. Q. Sun, S. J. Ding, and D. W. Zhang, “Band alignment and interfacial structure of ZnO/Si heterojunction with Al_2O_3 and HfO_2 as interlayers,” *Appl. Phys. Lett.*, vol. 104, no. 161602, 2014, doi: 10.1063/1.4872175.

[37] J. L. Alay and M. Hirose, “The valence band alignment at ultrathin SiO_2/Si interfaces,” *J. Appl. Phys.*, vol. 81, pp. 1606–1608, 1997.

[38] S. McNab, M. Yu, I. Al-Dhahir, E. Khorani, T. Rahman, S. A. Boden, P. P. Altermatt, P. R. Wilshaw, and R. S. Bonilla, “Alternative Dielectrics for Hole Selective Passivating Contacts and the Influence of Nanolayer Built-in Charge,” *AIP Conf. Proc.*, vol. 2487, no. 1, p. 020013 August, 2022, doi: 10.1063/5.0089282.

[39] M. Lei, J. H. Yum, S. K. Banerjee, G. Bersuker, and M. C. Downer, “Band offsets of atomic layer deposited Al_2O_3 and HfO_2 on Si measured by linear and nonlinear internal photoemission,” *Phys. Status Solidi Basic Res.*, vol. 249, no. 6, pp. 1160–1165, 2012, doi: 10.1002/pssb.201100744.

[40] T. Tan, Z. Liu, H. Lu, W. Liu, F. Yan, and W. Zhang, “Band structure and valence-band offset of HfO_2 thin film on Si substrate from photoemission spectroscopy,” *Appl. Phys. A Mater. Sci. Process.*, vol. 97, no. 2, pp. 475–479, 2009, doi: 10.1007/s00339-009-5245-8.

[41] V. V. Afanas’Ev, M. Houssa, A. Stesmans, C. Merckling, T. Schram, and J. A. Kittl, “Influence of Al_2O_3 crystallization on band offsets at interfaces with Si and TiN_x,” *Appl. Phys. Lett.*, vol. 99, 2011, doi: 10.1063/1.3623439.

[42] V. V. Afanas’ev, A. Stesmans, F. Chen, X. Shi, and S. A. Campbell, “Internal photoemission of electrons and holes from (100)Si into HfO_2,” *Appl. Phys. Lett.*, vol. 81, no. 6, pp. 1053–1055, 2002, doi: 10.1063/1.1495088.

[43] V. V. Afanas’ev, M. Houssa, A. Stesmans, and M. M. Heyns, “Electron energy barriers between (100)Si and ultrathin stacks of SiO_2, Al_2O_3, and ZrO_2 insulators,” *Appl. Phys. Lett.*, vol. 78, no. 20, pp. 3073–3075, 2001, doi: 10.1063/1.1366366.

[44] A. Schenk and G. Heiser, “Modeling and simulation of tunneling through ultra-thin gate dielectrics,” *J. Appl. Phys.*, vol. 81, no. 12, pp. 7900–7908, 1997, doi: 10.1063/1.365364.

[45] G. Dingemans, N. M. Terlinden, M. A. Verheijen, M. C. M. Van De Sanden, and W. M. M. Kessels, “Controlling the fixed charge and passivation properties of Si(100)/Al_2O_3 interfaces using ultrathin SiO2 interlayers synthesized by atomic layer deposition,” *J. Appl. Phys.*, vol. 110, no. 9, p. 093715, 2011, doi: 10.1063/1.3658246.

[46] M. L. Huang, Y. C. Chang, C. H. Chang, T. D. Lin, J. Kwo, T. B. Wu, and M. Hong, “Energy-band parameters of atomic-layer-deposition Al_2O_3/InGaAs heterostructure,” *Appl. Phys. Lett.*, vol. 89, no. 1, pp. 81–84, 2006, doi: 10.1063/1.2218826.

[47] K. M. Kim, J. S. Jang, S. G. Yoon, J. Y. Yun, and N. K. Chung, “Structural, optical and electrical properties of HfO_2 thin films deposited at low-temperature using plasma-enhanced atomic layer deposition,” *Materials (Basel).*, vol. 13, no. 9, pp. 1-10, 2020, doi: 10.3390/MA13092008.

[48] M. C. Cheynet, S. Pokrant, F. D. Tichelaar, and J. L. Rouvìre, “Crystal structure and band gap determination of HfO_2 thin films,” *J. Appl. Phys.*, vol. 101, no. 5, p. 054101, 2007, doi: 10.1063/1.2697551.

[49] Y. Jia, K. Zeng, J. S. Wallace, J. A. Gardella, and U. Singisetti, “Spectroscopic and electrical calculation of band alignment between atomic layer deposited SiO_2 and β-Ga_2O_3 ($2\bar{}01$),” *Appl. Phys. Lett.*, vol. 106, no. 10, pp. 2–5, 2015, doi: 10.1063/1.4915262.

[50] T. V. Perevalov, A. V. Shaposhnikov, V. A. Gritsenko, H. Wong, J. H. Han, and C. W. Kim, “Electronic structure of α-Al_2O_3: Ab initio simulations and comparison with experiment,” *JETP Lett.*, vol. 85, no. 3, pp. 165–168, 2007, doi: 10.1134/S0021364007030071.

[51] S. Monaghan, P. K. Hurley, K. Cherkaoui, M. A. Negara, and A. Schenk, “Determination of electron effective mass and electron affinity in HfO_2 using MOS and MOSFET structures,” *Solid. State. Electron.*, vol. 53, no. 4, pp. 438–444, 2009, doi: 10.1016/j.sse.2008.09.018.

[52] J. C. Garcia, L. M. R. Scolfaro, J. R. Leite, A. T. Lino, V. N. Freire, G. A. Farias, and E. F. Da Silva, “Effective masses and complex dielectric function of cubic HfO_2,” *Appl. Phys. Lett.*, vol. 85, no. 21, pp. 5022–5024, 2004, doi: 10.1063/1.1823584.

[53] A. Gehring and S. Selberherr, “Modeling of tunneling current and gate dielectric reliability for nonvolatile memory devices,” *IEEE Trans. Device Mater. Reliab.*, vol. 4, no. 3, pp. 306–319, Sep. 2004, doi: 10.1109/TDMR.2004.836727.

[54] B. Brar, G. D. Wilk, and A. C. Seabaugh, "Direct extraction of the electron tunneling effective mass in ultrathin SiO_2," *Appl. Phys. Lett.*, vol. 69, no. 18, pp. 2728–2730, 1996, doi: 10.1063/1.117692.

[55] W. C. Lee and C. Hu, "Modeling CMOS tunneling currents through ultrathin gate oxide due to conduction-and valence-band electron and hole tunneling," *IEEE Trans. Electron Devices*, vol. 48, no. 7, pp. 1366–1373, Jul. 2001, doi: 10.1109/16.930653.

[56] G. Kaur, Z. Xin, R. Sridharan, A. Danner, and R. Stangl, "Engineering aluminum oxide/polysilicon hole selective passivated contacts for high efficiency solar cells," *Sol. Energy Mater. Sol. Cells*, vol. 218, no. February, p. 110758, 2020, doi: 10.1016/j.solmat.2020.110758.

[57] C. Reichel, F. Feldmann, A. Richter, J. Benick, M. Hermle, and S. W. Glunz, "Polysilicon contact structures for silicon solar cells using atomic layer deposited oxides and nitrides as ultra-thin dielectric interlayers," *Prog. Photovoltaics Res. Appl.*, vol. 30, no. 3, pp. 288–299, 2022, doi: 10.1002/pip.3485.

[58] K. Gao, Q. Bi, X. Wang, W. Liu, C. Xing, K. Li, D. Xu, Z. Su, C. Zhang, J. Yu, D. Li, B. Sun, J. Bullock, X. Zhang, and X. Yang, "Progress and Future Prospects of Wide-Bandgap Metal-Compound-Based Passivating Contacts for Silicon Solar Cells," *Adv. Mater.*, vol. 34, no. 36, p. 2200344, 2022, doi: 10.1002/adma.202200344.

[59] A. B. Gougam, B. Rajab, and A. Bin Afif, "Investigation of c-Si surface passivation using thermal ALD deposited HfO_2 films," *Mater. Sci. Semicond. Process.*, vol. 95, no. 42–47, 2019, doi: 10.1021/acsomega.1c04793.

[60] A. Wratten, S. L. Pain, D. Walker, A. B. Renz, E. Khorani, T. Niewelt, N. E. Grant, and J. D. Murphy, "Mechanisms of Silicon Surface Passivation by Negatively Charged Hafnium Oxide Thin Films," *IEEE J. Photovoltaics*, vol. 13, pp. 40-47, 2023, doi: 10.1109/JPHOTOV.2022.3227624.

[61] D. Kang, H. C. Sio, J. Stuckelberger, D. Yan, S. P. Phang, R. Liu, T. N. Truong, T. Le, H. T. Nguyen, X. Zhang, and D. Macdonald, "Comparison of firing stability between p- and n-type polysilicon passivating contacts," *Prog. Photovoltaics Res. Appl.*, vol. 30, no. 8, pp. 970-980, 2022, doi: 10.1002/pip.3544.